588   *Bull. Korean Chem. Soc.* **2000**, Vol. 21, No. 6

Sunghyun Kim et al.

In situ Structural Investigation of Iron Phthalocyanine Monolayer Adsorbed on Electrode Surface by X-ray Absorption Fine Structure

Sunghyun Kim,[*] Toshiaki Ohta,[†] and Gwanghoon Kwag[‡]

Department of Chemistry, Konkuk University, Seoul 143-701, Korea
[†]Department of Chemistry, Graduate School of Science, The University of Tokyo, Tokyo 113-0033, Japan
[‡]Kumho Chemical Laboratories, Kumho Petrochemical Co., P.O. Box 64, Taejon 305-600, Korea
Received February 22, 2000

Structural changes of an iron phthalocyanine (FePC) monolayer induced by adsorption and externally applied potential on high area carbon surface have been investigated *in situ* by iron K-edge X-ray absorption fine structure (XAFS) in 0.5 M H_2SO_4. Fine structures shown in the X-ray absorption near edge structure (XANES) for microcrystalline FePC decreased upon adsorption and further diminished under electrochemical conditions. Fe(II)PC(-2) showed a 1s $\rightarrow$ 4p transition as poorly resolved shoulder to the main absorption edge rather than a distinct peak and a weak 1s $\rightarrow$ 3d transition. The absorption edge position measured at half maximum was shifted from 7121.8 eV for Fe(II)PC(-2) to 7124.8 eV for $[Fe(III)PC(-2)]^+$ as well as the 1s $\rightarrow$ 3d pre-edge peak being slightly enhanced. However, essentially no absorption edge shift was observed by the 1-electron reduction of Fe(II)PC(-2), indicating that the species formed is $[Fe(II)PC(-3)]^-$. Structural parameters were obtained by analyzing extended X-ray absorption fine structure (EXAFS) oscillations with theoretical phases and amplitudes calculated from FEFF 6.01 using multiple-scattering theory. When applied to the powder FePC, the average iron-to-phthalocyanine nitrogen distance, $d(Fe-N_p)$ and the coordination number were found to be 1.933 Å and 3.2, respectively, and these values are the same, within experimental error, as those reported (1.927 Å and 4). Virtually no structural changes were found upon adsorption except for the increased Debye-Waller factor of 0.005 $Å^2$ from 0.003 $Å^2$. Oxidation of Fe(II)PC(-2) to $[Fe(III)PC(-2)]^+$ yielded an increased $d(Fe-N_p)$ (1.98 Å) and Debye-Waller factor (0.005 $Å^2$). The formation of $[Fe(II)PC(-3)]^-$, however, produced a shorter $d(Fe-N_p)$ of 1.91 Å, the same as that of crystalline FePC within experimental error, and about the same Debye-Waller factor (0.006 $Å^2$).

Introduction

It has been well known that surfaces modified by foreign atomic and molecular species show very different physical and chemical properties from those of unmodified surfaces. They often, for example, promote the electron transfer rate and display catalytic behavior. It is therefore very important to elucidate the electronic and structural characteristics of these species induced by adsorption.[1] Many surface techniques down to monolayer sensitivity have been developed for this purpose, among which are X-ray photoelectron spectroscopy (XPS), low-energy electron diffraction (LEED), and electron energy loss spectroscopy (EELS). Unfortunately these methods cannot be applied to the interface where a liquid phase is involved. Measurements are only possible after the liquid phase is removed, which inevitably imposes an uncertainty for the surface state determination. However, the rather recent advent of synchrotron radiation has opened new prospects for the structural characterization of both crystalline and amorphous materials even in a solution phase, which was formerly inaccessible.[2-4] The intense, tunable X-ray can penetrate a thin layer of liquid to probe a solid-liquid interface. This technique has been adapted to the *in situ* study of electrode surfaces having a monolayer coverage.

In this paper, we present the electronic and structural determination of a FePC monolayer adsorbed on a carbon surface using XAFS as a function of potential. FePC (Figure 1) is a molecule that catalyzes many interesting reactions of fundamental and technological importance.[5-7] Reactants can bind to iron as an axial ligand and the electron transfer to and from the surface can occur. FePC shows two well-defined one-electron transfer processes in a consecutive manner. Although chemical and optical properties of FePC have been thoroughly studied in an aqueous phase, the relationships between electronic and structural aspects under the influence of potential are little known.[8-10] To study FePC monolayer behavior, we used carbon as an adsorbing substrate. The use of carbon is advantageous in XAFS experiments in that as a low-Z element, X-rays can freely penetrate it to probe the FePC molecules. This strategy has been successfully used in [57]Fe Mossbauer-effect spectroscopy.[11] Another merit of
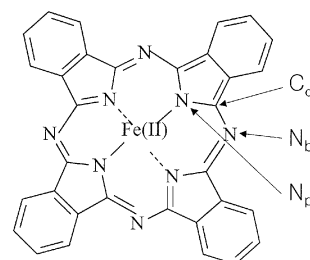

Figure 1. The structure of iron phthalocyanine, Fe(II)PC(-2). N_p, N_b, and C_α atoms are indicated.

using carbon is that it provides the FePC molecules with an equi-potential surface so that they are in the same oxidation state. We carried out both XANES and EXAFS to extract exact electronic and structural information.

Experimental Section

The adsorption of FePC was effected by adding 50 mg of high area carbon (Ketjen Black EC600JD (KB), 1360 m^2/g, Lion Corp., Japan), which was dispersed in methanol, to a solution of 20 mg of FePC dissolved in methanol. The mixture was ultrasonicated for 5 min, subjected to vigorous agitation for 1 h and then filtered using Whatman no. 2 filter paper. The filtrate was then washed with methanol until the filtrate solution was colorless. This material was dried in vacuum and stored under nitrogen at room temperature before use. All of the procedures were performed in a nitrogen-filled glove bag and care was taken to prevent the possible oxidation of FePC.

For electrochemical measurements, a small amount of FePC/KB was mixed with a drop of Teflon emulsion to increase the stickiness of the particles and applied to a carbon sheet (Karam Carbon, 0.3 mm thick, Korea). An ordinary electrochemical setup with a potentiostat (Pine RDE-5) and a three-electrode system (Ag/AgCl reference and Pt counter electrodes) was employed. Voltammograms were recorded using an X-Y recorder (Yokogawa, Japan).

All of the *in situ* experiments were carried out in the fluorescence mode with a cell schematically shown in Figure 2. The cell design was based on the literature with some modifications.[12,13] Compared with the previous design, the present cell does not have a thin layer geometry between the working electrode and the cell window. Thus, we avoided the ohmic polarization effect due to the large solution resistance. In this design, the working electrode also serves as a window. FePC-adsorbed carbon was applied to the carved section of *ca.* 5 × 15 mm^2 of a carbon sheet and only this section was exposed to electrolyte. Sealing was made by epoxy resin between the cell body made of Teflon and the working electrode. The electrical connection was directly made to the carbon sheet. Both reference and counter electrodes were placed in the bulk of the electrolyte out of the incoming beam path. The cell and the detector were mounted at 45° to the beam direction for the efficient detection of fluorescence.

Data Collection and Analysis

XAFS data were obtained at beam lines 3C1 at PLS (Pohang Light Source) and 7C at PF (Photon Factory), operating at 2.5 GeV with *ca.* 100-140 mA and 200-400 mA of stored current, respectively. A pair of Si(111) crystals was used as the monochromator. Powder samples were measured in the transmission mode with ion chamber detectors while the Lytle-type detector was used for the *in situ* fluorescence measurements with a Mn filter of a three absorption lengths interposed between the detector and the cell. The higher har-
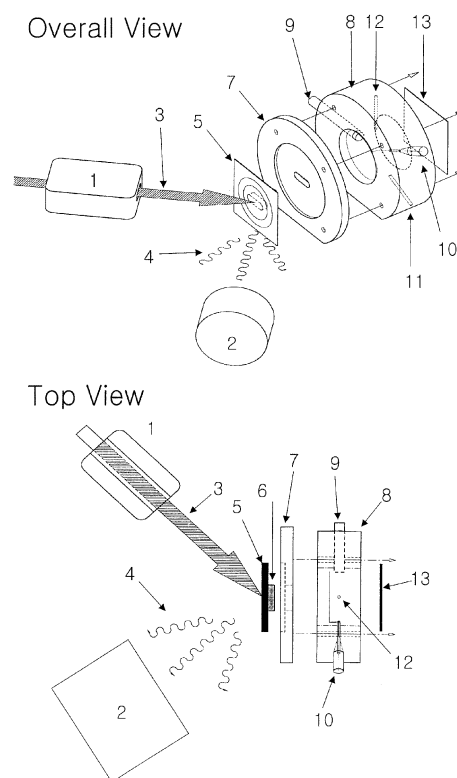

Figure 2. Schematic diagram of the *in situ* spectroelectrochemical cell used in this experiment. 1: ion chamber detector, 2: Lytle detector, 3: incident X-ray beam, 4: X-ray fluorescence 5: carbon sheet, 6: FePC/KB 7: cell cover, 8: cell body, 9: reference electrode, 10: counter electrode, 11: solution inlet 12: solution outlet, 13: Kapton tape.

monics contained in the incident beam intensity, I_0, were minimized by detuning the crystals to pass about 80% of the maximum I_0. The XANES region was scanned at equal energy steps of 0.30 eV/point to resolve fine structures. The EXAFS spectrum was obtained at energy intervals of constant photoelectron wave vector k, 0.05 Å^{-1}. A rather rapid scanning scheme was used in the XANES region while time averaging up to *ca.* 10 s/point was made in the EXAFS region to increase the S/N ratio. An iron foil of three absorption lengths was used to calibrate the energy before and after the experiments. 7112 eV was used as an energy reference, E_0.

The primary XAFS data, $Ln(I_0/I_t)$ for the transmission and I_f/I_0 for the fluorescence measurements, were normalized after extending the pre-edge region to the post-edge region using the Victoreen formula. EXAFS was extracted from the normalized XAFS spectra, after converting from eV to k-space by the equation, $k = \sqrt{0.263(E - E_0)}$, and fitting with a routine (AUTOBK) provided in the UWXAFS package[14] (version 3.0). The EXAFS, $\chi(k)$, is described by the following equation,

$$\chi(k) =$$

$$\sum_R N_R S_0^2 \frac{f_{eff}}{kR^2} \sin(2kR + \phi(k)) \exp(-2k^2\sigma^2) \exp(-2R/\lambda).$$

Parameters of our primary interest are the absorber-scatterer distance, R, the number of scattering atoms, N_R, and the Debye-Waller factor, σ^2. S_0, f_{eff}, $\phi(k)$, and λ are reduction factor, effective backscattering amplitude, phase shift, and electron mean free path, respectively. We multiplied $\chi(k)$ by k^3 to enhance the oscillatory part at high k. We put our emphasis on the first shell only as the most reliable information could be attained, although the second and third shells can be analyzed for powder samples. We assumed that the nearest neighbor is nitrogen and tried to fit higher shells beyond the first shell whenever necessary. Theoretical phase and backscattering amplitude as a function of k were calculated from FEFF 6.01 using multiple scattering theory.[15,16] R, N_R, σ and E_0 were allowed to float for the best fitting. Fitting results were displayed in both k- and R-space.

Results and Discussion

Figure 3 is a cyclic voltammogram of FePC adsorbed on KB in 0.5 M H_2SO_4. Two reversible redox peaks at +0.40 V and -0.08 V are due to the consecutive 1-electron transfer processes corresponding respectively to $[Fe(III)Pc(-2)]^+ + e^- \leftrightarrow Fe(II)PC(-2)$ and $Fe(II)PC(-2) + e^- \leftrightarrow [Fe(II)PC(-3)]^-$. Figures 4 and 5 show *in situ* normalized and first differential XANES at three different oxidation states of FePC, including powder spectra. XANES of microcrystalline FePC (Figure 4, curve A) shows several fine structures labeled 1 to 5. The first peak, barely visible, which is found in most transition metals of unfilled d-orbitals, has been assigned to the 1s $\rightarrow$ 3d transition. This transition is forbidden by the dipole selection rule but allowed from the quadrupole-selection rule by the orbital mixing between metallic d- and ligand p-character. The weakness of this peak indicates that FePC possesses high symmetry, D_{4h}. The other transitions (2-5) all involve iron 4p orbitals. As for CoPC,[17] these peaks are assigned as follows: a shake-down satellite involving 1s $\rightarrow$ 4p$_z$ (peak 2), pure 1s $\rightarrow$ 4p$_z$ transitions (peaks 3 and 4), and a 1s $\rightarrow$ 4p$_{xy}$ transition (peak 5). All of these features are diminished when XANES was taken on the FePC-adsorbed carbon powder (curve B). Comparing curves A and B in Fig-
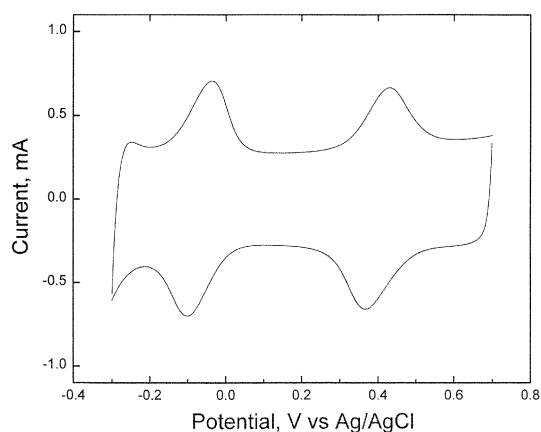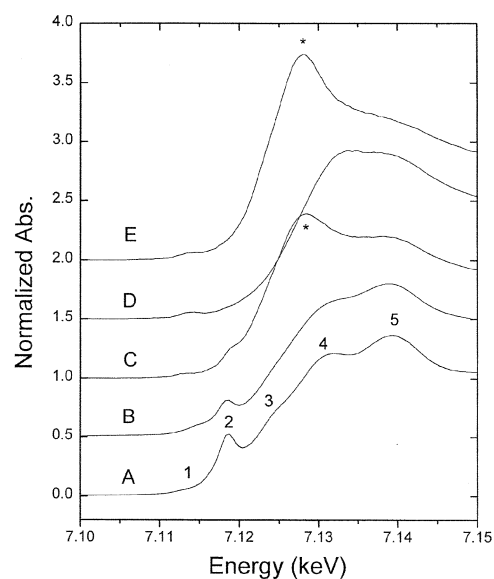

Figure 4. Normalized Fe K-edge XANES spectra: FePC in microcrystalline (A) and adsorbed (B) states. Curves C-E are *in situ* results of Fe(II)PC(-2), [Fe(III)PC(-2)]$^+$, and [Fe(II)PC(-3)]$^-$, respectively. The vertical scale is offset for clarity.

ures 4 and 5, several things are noticeable. There was a small enhancement in the 1s $\rightarrow$ 3d transition (peak 1) with a simultaneous decrease in transition 2. At least two factors are responsible for this observation. (i) Some FePC molecules may be distorted upon adsorption so that D_{4h} symmetry is no longer maintained. (ii) More plausibly, part of the FePC was oxidized to form the μ-oxo derivative of FePC, $(FePC)_2O$, having a square-pyramidal symmetry, because FePC is known to be easily oxidized in air.

Curves C, D, and E are XANES of FePC obtained after several potential cycles between -0.3 V and +0.7 V. At +0.2 V where the Fe(II)PC(-2) species exists, the XANES looks quite different from that of microcrystalline FePC although
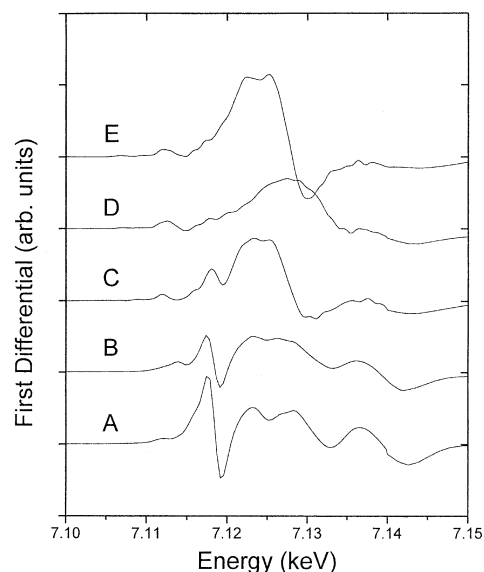

Figure 3. Cyclic voltammetry of FePC/KB in 0.5 M sulfuric acid. Scan rate: 10 mV/s.

Figure 5. First differential XANES spectra for the data shown in Figure 4.

the formal oxidation state of iron is the same (curve C). Most fine structures are greatly diminished: the 1s → 4p$_z$ transition (peak 2) appears as a shoulder, not a distinct peak on the main absorption edge, and transitions 3 and 4 are not resolved but merged into a sharp white line labeled as *. Transition 5 is still clear. The loss of fine structures is caused by exposure of FePC to the electrolyte, where the axial ligation of water molecules forms an octahedral $(H_2O)_2Fe(II)$-PC(-2). Water molecules could donate electrons to the empty 4p orbitals of iron, resulting in diminution of the 1s → 4p transition. The oxidation state of iron could be inferred from the position of the 1s → 3d transition. This transition has been used to determine the formal oxidation state of transition metals such as V,[18] Mn,[19] Ni[20] and Mo.[21] as well as S.[22] Kunzl's law[23] states that the pre-edge position is linearly related to the formal valence of the element. The positive shift in energy as the valency increases is due to the increase in the attractive potential of the nucleus on the 1s electrons. Approximately 1 eV difference is observed for each valency change. The 7111.9 eV value for Fe(II)PC(-2) is exactly the same as that of microcrystalline FePC.

A large change was observed when the electrode was polarized at +0.6 V to form $[Fe(III)Pc(-2)]^+$ (curve D). Most noticeable are the disappearance of the pre-edge peak at 7118.0 eV (peak 2) and the shift of the absorption edge position toward higher energy, to 7124.8 eV from 7121.8 eV, as well as an increased pre-edge peak at 7112.7 eV (peak 1). The fact that the position of the pre-edge determined from the first differential spectrum is almost identical with that of the reference sample, Fe_2O_3 indicates that the iron center is fully oxidized to the trivalent state. The larger pre-edge peak at 7112.7 eV implies that the molecular geometry deviates from D_{4h} symmetry. The formation of the dimeric μ-oxo species, $[Fe(III)PC(-2)]_2O$ may not be possible because the peak intensity is much smaller than that of $[FePC]_2O$ (data not shown), and there is no report for the existence of the μ-oxo species in strongly acidic conditions. Further distortion of the structure upon oxidation of iron is more plausible. However, the interconversion of monomer and μ-oxo dimeric species has been observed in (μ-oxo)bis[iron *meso*-tetrakis(4-methoxyphenyl)porphyrin], $[Fe(TMPP)]_2O$,[24] in neutral solutions, causing an increased $d(Fe-N_p)$.

Virtually no changes have been made when polarizing the electrode at -0.20 V (curve E). Almost the same XANES as the one at +0.2 V (curve C) was obtained. The positions of the 1s → 3d transition and the main absorption edge appeared at almost the same energies as those of Fe(II)PC (-2), strongly indicating that $[Fe(II)PC(-3)]^-$ possesses a similar structure with Fe(II)PC(-2) and iron remains in a divalent state. Some differences are found, however: the 1s → 4p$_z$ transition appeared at 7118.0 eV (peak 2) became negligible and the white line labeled * was enhanced. In general, an increase in the density of an unoccupied final state, *i.e.*, the oxidation of an absorbing atom, causes an increase of the white line intensity, especially in the L$_{III}$-edges of various 5d metals[25] and Ni K-edge.[26] In our case, it is not certain at the moment why $[Fe(II)PC(-3)]^-$ shows higher white line inten-

Table 1. Fe K-edge positions in eV for FePC under various conditions

Compound	1s → 3d^a	1s → 4p$_z$^{a}	$E_{\mu t=0.5}$^{b}
FePC microcrystalline	7111.9	7117.5	7122.4
FePC/KB	7113.6	7117.4	7123.3
$[Fe(III)PC(-2)]^+$	7112.7		7124.8
Fe(II)PC(-2)	7111.9	7118.0	7121.8
$[Fe(II)PC(-3)]^-$	7111.9		7121.4

^{a}Measured as the energy of the inflection point. ^{b}Measured as the energy at which the normalized absorption is equal to 0.5.

sity. The result at least rules out the possibility of iron being reduced to the +1 oxidation state, because that should result in either no change or a diminution of the white line. Changes in ionic environment around the FePC molecules may cause this phenomenon as noted in ref. 27. The injected electron is believed to go to an empty $e_g(\pi^*)$ orbital,[28] mostly of PC ring character to make $[Fe(II)PC(-3)]^-$. Table 1 lists various Fe K-edge positions for the spectra shown in Figure 4.

Detailed structural information could be obtained from the EXAFS analysis. Figures 6 to 10 are k^3-weighted EXAFS spectra and the corresponding Fourier transforms and fitting results. The solid lines (Panel A in Figures 7 and 8) exhibit the characteristic peak pattern of FePC obtained from curves A and B in Figure 6. In each FT plot, the first strong peak at *ca.* 1.5 Å (before phase shift correction) is due to backscattering from the four N$_p$ atoms. The second peak at *ca.* 2.5 Å and the shoulder at 3.2 Å are due to backscattering from the eight carbon atoms of the pyrrole ring bonded to nitrogen, C$_\alpha$, and the four bridging nitrogen, N$_b$ atoms, respectively. For the structural determination, the curve-fitting has been done over the range from 0.5 Å to 3.5 Å by applying the Hanning window, employing multiple-scattering theory. The fitting results are displayed as dotted curves in both R and k-
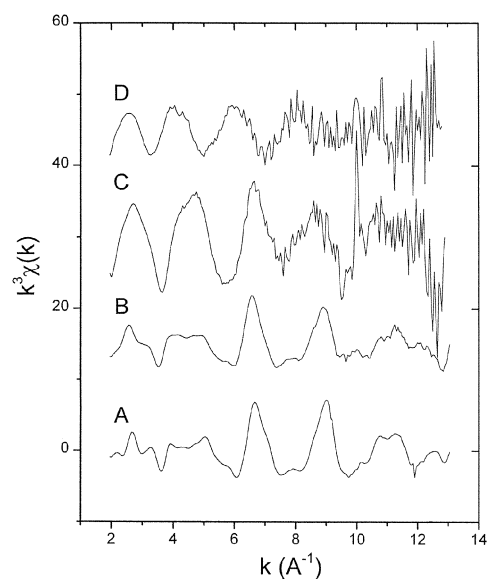

Figure 6. Background-subtracted Fe K-edge EXAFS, $k^3\chi(k)$, for FePC in microcrystalline (A), adsorbed (B) states, and for $[Fe(III)PC(-2)]^+$ (C) and $[Fe(II)PC(-3)]^-$ (D).
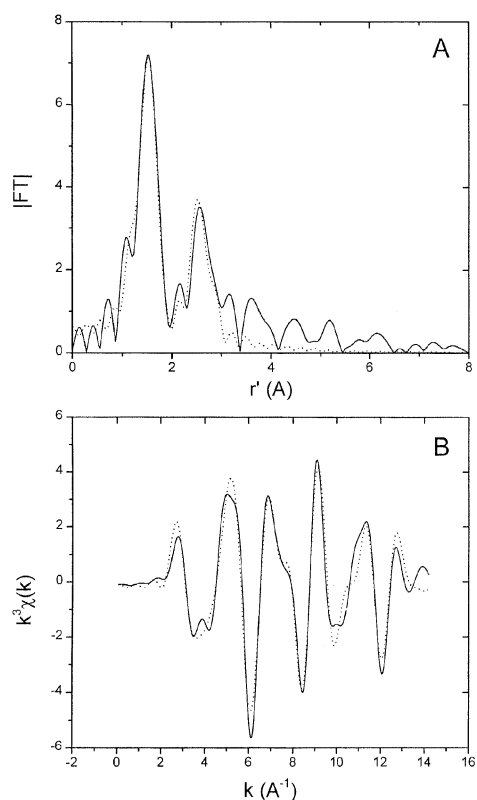
592 *Bull. Korean Chem. Soc.* **2000**, Vol. 21, No. 6

Sunghyun Kim et al.

Figure 7. FT (solid line, Panel A) for EXAFS of microcrystalline FePC shown in curve A, Figure 6 and corresponding Fourier-filtered back-FT (solid line, Panel B) spectra. Dotted lines are fitted results in *R*- (Panel A) and *k*-spaces (Panel B).
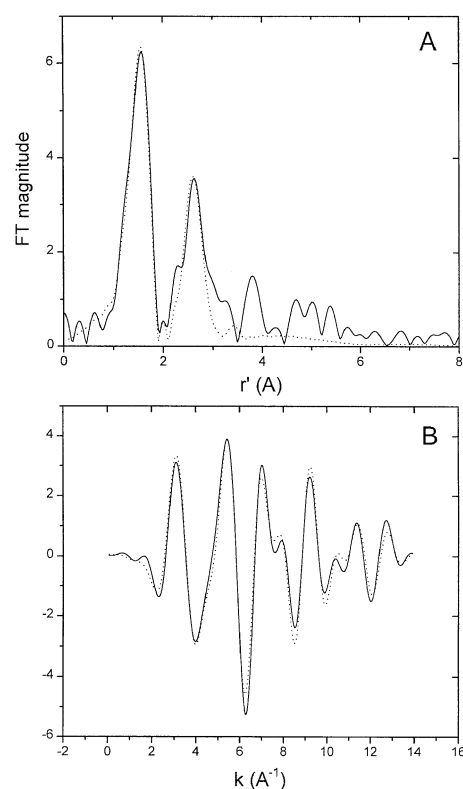

Figure 8. FT (solid line, Panel A) for EXAFS of adsorbed FePC shown in curve B, Figure 6 and corresponding Fourier-filtered back-FT (solid line, Panel B) spectra. Dotted lines are fitted results in *R*- (Panel A) and *k*-spaces (Panel B).

space (Panel B). Although good agreement between theory and data has been obtained, we confined our analysis only to the first shell. Fitting beyond the first shell may cause erroneous results for the *in situ* data. We obtained 1.933 Å of d(Fe-N$_p$) for FePC both in microcrystalline and adsorbed states. This is in good agreement with the reported value of 1.927 Å for FePC, confirming the validity of our analysis. The Debye-Waller factor for adsorbed FePC (0.005 Å^2) was somewhat larger than that of microcrystalline FePC (0.003 Å^2). This indicates that molecular relaxation has taken place upon adsorption and explains some loss of fine structure in the XANES. Coordination numbers were calculated to be 3.2 and 3.0 for microcrystalline and adsorbed FePC, respectively, which are not significantly different from 4. Table 2 summarizes the fitting results for powder samples and *in situ* data.

All *in situ* EXAFS data are rather noisy due to the small amount of FePC confined on the electrode surface and the scattering effect of the electrolyte, (curves C and D in Figure 6). Nevertheless, it is possible to analyze the first shell. [Fe(III)PC(-2)]$^+$ shows a very distinct first shell and a small second shell. The best fitted values for d(Fe-N$_p$), N_R, and σ are 1.98 Å, 5.5, and 0.005 Å^2, respectively. The iron-to-nitrogen distance is slightly longer than that of pure and adsorbed FePC. This is believed to be caused by distortion of the molecule by oxidation, which was also evidenced by the enhanced 1s → 3d peak in the XANES. The formation of

Table 2. Curve fitting results for the Fourier filtered $k^3\chi(k)$ Fe K-edge EXAFS of FePC under various conditions

Compounds	d(Fe-N$_p$), Å	N_R	σ^2, Å^2
FePC microcrystalline	1.93	3.2	0.003
FePC/KB	1.93	3.0	0.005
[Fe(III)PC(-2)]$^+$	1.98	5.5	0.005
[Fe(II)PC(-3)]$^-$	1.91	3.8	0.006

Note: The backscattering amplitudes and phase shifts were obtained from FEFF 6.01. Δk ranges were 10.5 Å^{-1} for *in situ* data and 11 Å^{-1} for the powder samples over which the fitting was performed. *In situ* results for Fe(II)PC(-2) were not listed due to the noisy nature of EXAFS. The uncertainty in d(Fe-N$_p$) is about ± 0.02 Å.

dimeric μ-oxo species may not be possible for reasons discussed in the XANES section. Iron tetrakis(4-methoxyphenyl)porphyrin, FeTMPP,[24] shows similar behavior in acidic conditions. Once the μ-oxo species formed, d(Fe-N$_p$) increased by 0.06 Å in this case, as well as the shoulder to the Fe-N$_p$ shell at low r in the FT spectrum. In our case, there is no indication of a shoulder peak and the fitting result was good without assuming an additional shell. The N_R obtained is a reasonable good value as a coordination number and not much stress has been placed on it. The increased Debye-Waller factor indicates that the FePC molecules undergo much molecular relaxation due to adsorption and exposure to the electrolyte.

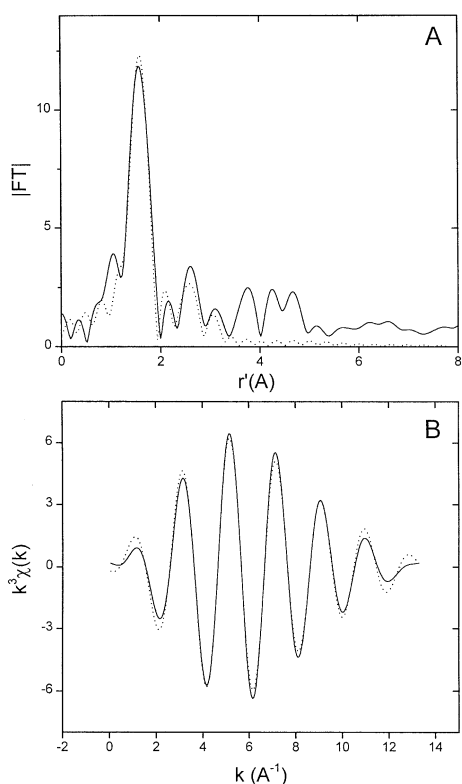The case of [Fe(II)PC(-3)]$^-$ is rather peculiar in that the FT

Figure 9. FT (solid line, Panel A) for EXAFS of $[Fe(III)PC(-2)]^+$ shown in curve C, Figure 6 and corresponding Fourier-filtered back-FT (solid line, Panel B) spectra. Dotted lines are fitted results in R- (Panel A) and k-spaces (Panel B).
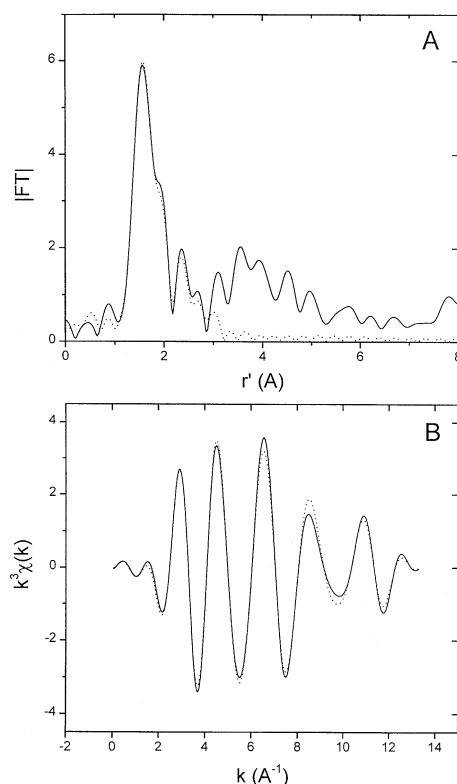

Figure 10. FT (solid line, Panel A) for EXAFS of $[Fe(II)PC(-3)]^-$ shown in curve D, Figure 6 and corresponding Fourier-filtered back-FT (solid line, Panel B) spectra. Dotted lines are fitted results in R- (Panel A) and k-spaces (Panel B).

spectrum shows a rather pronounced shoulder on the Fe-N_p shell (Panel A, Figure 10). The single shell fitting gave only poor results. The interatomic distance obtained, 2.04 Å, is unreasonably large for d(Fe-N_p). Since the r' position of the shoulder peak appears below that of Fe-C_α shell, we assume that water molecules are bonded to iron as axial ligands. Although no crystal structure of $[FePC(OH_2)_2]^-$ has not been reported, a non-μ-oxo complex having water molecules as axial ligands can be found in iron porphyrin, [Fe(TPP)-$(OH_2)_2]^+$.[29] The average iron-to-ligand distances are 2.045 for d(Fe-N_p) and 2.095 Å for d(Fe-O). In our case, the difference (=d(Fe-O)-d(Fe-N_p)) for $[FePC(OH_2)_2]^-$ seems much larger from the FT spectrum. It is generally accepted that shells separated by less than $\pi/2\Delta k$ cannot be resolved. With Δk of 10.5 Å^{-1} in this analysis, the minimum distance should be larger than *ca*. 0.16 Å. At any rate, we proceeded with a two-shell fitting. However, we did not extensively pursue the search for axial ligands. The best fitted value of 1.91 Å for d(Fe-N_p) is the same as the crystalline value within experimental error, indicating that the FePC structure is maintained. The N_R of 3.8 also implies that four nitrogen atoms are coordinated to iron. The increased Debye-Waller factor of 0.006 Å^2 indicates the same kind of molecular relaxation as in $[Fe(III)PC(-2)]^+$ taking place.

Conclusions

In this paper we have demonstrated how X-ray absorption

spectroscopy could be applied *in situ* to electrochemistry to study structural and electronic aspects of FePC adsorbed on an electrode surface. In combination with cyclic voltammetry, *in situ* XANES and EXAFS studies yielded the following results. (i) The adsorption of FePC and the exposure to electrolyte gives rise to a molecular relaxation, leading to diminution in fine structure and larger Debye-Waller factors as a result. (ii) The formation of $[Fe(III)PC(-2)]^+$ lowers the molecular symmetry and causes a large absorption edge shift toward higher energy. (iii) $[Fe(II)PC(-3)]^-$ is formed when reducing Fe(II)PC(-2) with no change in absorption edge position. (iv) The iron-to-nitrogen distance does not change within experimental error under electrochemical conditions.

The present work shows that XAFS can be a useful tool for the *in situ* study of structural aspects of adsorbed species in electrochemical cells. More detailed information beyond the first shell may be available with higher quality data, which can be obtained with a better cell design and detection system.

References

1. For a collection of monographs in the area of *in situ* appli-

cations to spectroscopic techniques to the study of electrode-electrolyte interfaces, see: *Spectroelectrochemistry: Theory and Practices*; Gale, R., Ed.; Plenum Press: New York, 1988.

2. *Electrochemical Interfaces: Modern Techniques for in situ Interface Characterization*; Abruna, H. D., Ed.; VCH Publishers: New York, 1991.

3. *Investigations of Surfaces and Interfaces*; Rossiter, B. W., Baetzold, R. C., Eds.; *Physical Methods in Chemistry*, 2nd ed.; John Wiley & Sons Inc.: New York, 1993; Vol IXB.

4. Sharpe, L. R.; Heineman, W. R.; Elder, R. C. *Chem. Rev.* **1990**, *90*, 705.

5. Van der Brink, F.; Barendrecht, E.; Visscher, W. *Recl.: J. R. Neth. Chem. Soc.* **1980**, *99*, 253.

6. Applyby, A. J.; Savy, M.; Caro, P. *J. Electroanal. Chem.* **1980**, *111*, 91.

7. Tanaka, A. A.; Fierro, C.; Scherson, D.; Yeager, E. *Mat. Chem. Phys.* **1989**, *22*, 431.

8. Zagal, J.; Bindra, P.; Yeager, E. *J. Electrochem. Soc.* **1980**, *127*, 1506.

9. Elzing, A.; van der Putten, A.; Visscher, W.; Barendrecht, E. *J. Electroanal. Chem.* **1987**, *233*, 99.

10. Nevin, W. A.; Liu, W.; Melnik, M.; Lever, A. B. P. *J. Electroanal. Chem.* **1986**, *213*, 217.

11. Fierro, C. A.; Mohan, M.; Scherson, D. *Langmuir* **1990**, *6*, 1338.

12. Kim, S.; Bae, I. T.; Sandifer, M.; Ross, P. N.; Carr, R.; Woicik, J.; Antonio, M. R.; Scherson, D. A. *J. Am. Chem. Soc.* **1991**, *113*, 9063.

13. Tryk, D. A.; Bae, I. T.; Hu, Y.; Kim, S.; Antonio, M. R.; Scherson, D. A. *J. Electrochem. Soc.* **1995**, *142*, 824.

14. UWXAFS Project, Department of Physics, FM-15, University of Washington, Seattle, WA 98159, USA.

15. Rehr, J. J.; Albers, R. C. *Phys. Rev.* **1990**, *B41*, 8139.

16. Rehr, J. J.; Zabinsky, S. I.; Albers, R. C. *Phys. Rev. Lett.* **1992**, *69*, 3397.

17. Martins Alves, M. C.; Dodelet, J. P.; Guay, D.; Ladouceur, M.; Tourillon, G. *J. Phys. Chem.* **1992**, *96*, 10898.

18. Wong, J.; Lytle, F. W.; Messmer, R. P.; Maylotte, D. H. *Phys. Rev. B* **1984**, *30*, 5596.

19. Liu, R. S.; Jang, L. Y.; Chen, J. M.; Tsai, Y. C.; Hwang, Y. D.; Liu, R. G. *J. Solid State Chem.* **1997**, *128*, 326.

20. Mansour, A. N.; Melendres, C. A.; Pankuch, M.; Brizzolara, R. A. *J. Electrochem. Soc.* **1994**, *141*, L69.

21. Cramer, S. P.; Eccles, T. K.; Kutzler, F. W.; Hodgson, K. O. *J. Am. Chem. Soc.* **1975**, *98*, 1287.

22. George, G. N.; Gorbaty, M. L. *J. Am. Chem. Soc.* **1989**, *111*, 3182.

23. Kunzl, V. *Collect Trav. Chim. Tschoselovaquie* **1932**, *4*, 213.

24. Kim, S.; Tryk, D. A.; Bae, I. T.; Sandifer, M.; Carr, R.; Antonio, M. R.; Scherson, D. A. *J. Phys. Chem.* **1995**, *99*, 10359.

25. Sinfelt, J. H.; Meitzner, G. D. *Acc. Chem. Res.* **1993**, *26*, 1.

26. Jentys, A.; Haller, G. L.; Lercher, J. A. *J. Phys. Chem.* **1992**, *96*, 1324.

27. *X-ray Absorption Fine Structure for Catalysts and Surfaces*; Iwasawa, Y., Ed.; World Scientific Co.: Singapore, 1996.

28. Fierro, C.; Anderson, A. B.; Scherson, D. *J. Phys. Chem.* **1988**, *92*, 6902.

29. Scheidt, W. R.; Cohen, I. A.; Kastner, M. E. *Biochemistry* **1979**, *18*, 3546.